Applied Energy 341 (2023) 121068

Contents lists available at ScienceDirect

Applied Energy

journal homepage: www.elsevier.com/locate/apenergy

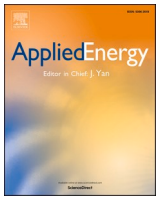

Polymeric stabilization of salt hydrates for thermochemical energy storage

Joey Aarts [a,b], Bas van Ravensteijn [c], Hartmut Fischer [d], Olaf Adan [b,d], Henk Huinink [a,b,*]

[a] Eindhoven Institute of Renewable Energy Systems, Eindhoven University of Technology, PO Box 513, Eindhoven 5600 MB, the Netherlands
[b] Transport in Permeable Media Group, Department of Applied Physics, Eindhoven University of Technology, PO Box 513, Eindhoven 5600 MB, the Netherlands
[c] Utrecht University, Department of Pharmaceutical Sciences, Universiteitsweg 99, 3584 CG Utrecht, the Netherlands
[d] TNO Materials Solution, High Tech Campus 25 Eindhoven, the Netherlands

HIGHLIGHTS

- Salt hydrates can be stabilized by impregnation into a highly porous polymer matrix.
- Poly-HEMA can stabilize various salts undergoing hydration and deliquescence.
- Due to the flexible matrix higher deliquescence water vapor pressures can be used.
- Flexible polymers have high potential for salt hydrate stabilization.
- Hydration kinetics improve over hydration and dehydration cycles.

GRAPHICAL ABSTRACT

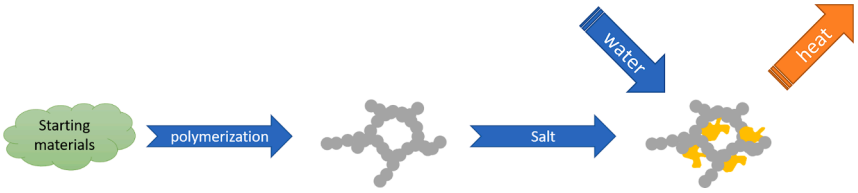

ARTICLE INFO

Keywords:
Salt hydrates
Thermochemical energy storage
Polymers
Stabilization
Kinetics
Cyclic stability

ABSTRACT

Non-stabilized thermochemical materials impose several limitations on their use. These include swelling/shrinkage, cracking, and agglomeration over cycles. In addition, the deliquescence transition cannot be used and is even considered an unwanted side effect. In this work several salt hydrates for low temperature heat storage (K_2CO_3, $CaCl_2$ and LiCl) are stabilized within a highly porous mm-sized polymer matrix. The composites containing wetting salt solutions are shown to be stable towards deliquescence. Three different composites were cycled. A K_2CO_3-polymer composite was cycled for 50 hydration/dehydration cycles and found to be kinetically and mechanically stable over all cycles, with swelling at higher cycle numbers. A LiCl-polymer composite was cycled for 40 cycles after which the composite became unstable. The composite containing $CaCl_2$ was found to be kinetically and mechanically stable for 15 cycles. Composites with energy densities up to 2.4 $GJ{\cdot}m^{-3}$ and a peak power output of 325 $W{\cdot}kg^{-1}$ were fabricated which is equal or higher compared to previously reported systems. All composites have power outputs which are sustained at higher levels throughout the full discharge cycle. This work opens new pathways to stabilize salt hydrates as well-defined mm-sized particles exhibiting cyclic stability, while maintaining a high energy density and power output.

* Corresponding author at: Eindhoven Institute of Renewable Energy Systems, Eindhoven University of Technology, PO Box 513, Eindhoven 5600 MB, the Netherlands.
E-mail addresses: j.aarts@tue.nl (J. Aarts), b.g.p.vanravensteijn@uu.nl (B. van Ravensteijn), hartmut.fischer@tno.nl (H. Fischer), olaf.adan@tno.nl (O. Adan), h.p.huinink@tue.nl (H. Huinink).

https://doi.org/10.1016/j.apenergy.2023.121068
Received 5 December 2022; Received in revised form 6 March 2023; Accepted 29 March 2023
Available online 19 April 2023

1. Introduction

To achieve a net-zero carbon emission by the end of 2050, energy production needs to transition from the use of fossil fuels towards using renewable energy sources [1]. Since the direct use of renewables, such as solar or wind energy, is location and time dependent, thermochemical energy storage (TCES) can be used as a loss-free heat storage technology. One class of TCES uses salt hydrates, which release energy when exposed to water vapor. This energy release can occur due to hydration or deliquescence of the salt [2,3]. Hydration proceeds via incorporation of water molecules in the crystal lattice and is governed by the following chemical equation

$$\mathrm{salt(s)} + \alpha \mathrm{H_2O\,(g)} \rightleftharpoons \mathrm{salt}\cdot\beta\,\mathrm{H_2O\,(s)} + (\alpha-\beta)\,\mathrm{H_2O\,(g)}. \quad [1]$$

Where $\alpha[-]$ and $\beta[-]$ represent the stochiometric coefficients of the reaction. In the case of deliquescence, the vapor pressures are so high that the salt starts to dissolve in its absorbed water forming a saturated solution. Higher water vapor pressures will result in dilution of the saturated solution [4]. The corresponding chemical equation is

$$\mathrm{salt\,(s)} \xrightarrow{\mathrm{H_2O\,(g)}} \mathrm{salt\,(aq)}. \quad [2]$$

The usage of salt hydrates for TCES has several limitations, when used as the non-stabilized and pure material. One of these limitations is that the vapor pressures at which the salt can be used are limited to vapor pressures below the deliquescence pressures at which the salt starts to form a saturated solution. In addition, during consecutive (de) hydration cycles salt hydrates typically undergo swelling/shrinkage, cracking and agglomeration [5].

To overcome these limitations several attempts have been made to stabilize various salt hydrates. Stabilization can generally be achieved according to three methods: stabilization by encapsulation, stabilizing the salt inside a porous matrix and salt-binder composites. Stabilizing the salt inside a porous matrix has the main advantage that deliquescent transition can be used which is accompanied by high water uptake and higher energy densities compared to the hydration transition. A brief number of stabilization methods found in literature are listed in Table 1.

Some challenges exist when considering the literature examples in Table 1. Many of the cited literature examples are mainly focused on stabilizing salt hydrates in small powder or irregular granules/particles. For the application inside a thermochemical reactor an additional manufacturing step is necessary to convert the stabilized material into well-defined mm-sized particles. Otherwise large pressure drops over the thermochemical reactor bed will occur due to poor diffusion and flowability throughout the bed [25]. This results in a low power output of the reactor bed. On the other hand, mm-sized particles have some drawbacks as well. It was already shown by Shkatulov and coworkers that in the case of irregular granules the poor packing of the vermiculite stabilized K_2CO_3 composite resulted in an additional decrease in volumetric storage density (VSD) by a factor 2 [12]. In addition, manufacturing of powder into larger shape stable, and well-defined particles, can significantly reduce the material performance due to possible diffusion limitations as discussed recently [26]. Recent literature on flexible polydimethylsiloxane (PDMS)-salt foams shows promising results in terms of composite fabrication, mechanical integrity and hydration properties [21,22,23,24]. However, no flexible foams providing stability during both hydration and deliquescent cycling have been reported.

Table 1
Literature examples of several stabilization attempts of salt hydrates.

Salt	Stabilization method	Reference
K_2CO_3	Polymeric coatings	[6]
LiCl, $CaCl_2$ and $SrBr_2$	Hollow SiO2 spheres	[7]
$CaCl_2$	Microencapsulation using ethyl cellulose	[8]
$CaCl_2$, $MgSO_4$, $Ca(NO_3)$, $Li(NO_3)$ and LiBr	Silica gel, vermiculite, activated carbon and zeolite 13X	[9,10]
$MgCl_2$ and $MgSO_4$	Zeolite	[11]
K_2CO_3	Vermiculite	[12]
LiCl	Silica gel	[13]
$SrCl_2$	Expanded clay and Pumice	[14]
$CaCl_2$, $MgCl_2$ and $SrCl_2$	Silica gel	[15]
$MgSO_4$	Zeolite	[16]
$CaCl_2$	Bentonite	[16,17]
$CaCl_2$	Silica gel	[17]
$CaCl_2$	Attapulgite	[18]
$CaCl_2$	Alumina	[17]
LiCl	Activated alumina	[19]
$CaCl_2$	Expanded natural graphite and vermiculite	[8]
$SrCl_2$	Graphite and polyelectrolyte composite	[20]
$MgSO_4$	Polydimethylsiloxane (PDMS)	[21,22,23]
LiCl	Polydimethylsiloxane (PDMS)	[24]

Stabilization of the salt hydrate should be performed on well-defined millimeter length scale objects which meet the following criteria:

1. The stabilized material should enable a good airflow throughout the reactor bed.
2. The energy density should be comparable to irregular particles.
3. The power output must be high.

From these three criteria numbers 1 and 3 are the most critical ones, since systems with a high energy density and low power output are not suitable for thermal energy storage. This way, the stabilized material will be directly available for heat storage applications without any further processing steps that potentially limit the maximum achievable power output.

In this work, a porous hydrophilic polymeric matrix based on poly (hydroxyethyl methacrylate) (pHEMA) crosslinked with *N*,*N*′- methylene bisacrylamide (MBAA) is used to stabilize the salt hydrates. pHEMA is used in various biomedical applications such as the world's first contact lenses [27], bone tissue generation, wound healing, cancer therapy [28] and artificial skin [29]. In this work a macroscopic super porous monolithic structure was fabricated according to the method described in the work of Kovačič et al. [30]. This monolithic structure is used in this work as the stabilizing matrix. The main advantages are that the shape and size can be precisely controlled by the polymerization molds whereas the matrix properties such as porosity and pore size distribution can be tuned by changing the polymerization reaction or polymer composition. Highly porous pHEMA-*co*-MBAA has been shown to have excellent water sorption capabilities due to the polymer hydrophilicity and capillary action [31]. pHEMA is flexible and able to swell in solution without dissolving due to crosslinking [32]. This potentially provides additional deliquescence stability above the deliquescence relative humidity (DRH) as swelling accommodates the additional water volume. Therefore, higher storage densities are expected, when utilizing the deliquescence transition compared to rigid matrices, since higher water vapor pressures in combination with high salt content can be used without leakage. Furthermore it is non-toxic and has a high fracture resistance [28]. These material properties, combined with easy processability, make it a potential candidate for stabilizing salt hydrates.

In this study, six widely considered salt candidates were selected and tested. K_2CO_3, LiCl, $CaCl_2$ and $MgCl_2$ were selected based on a screening by Donkers et al. in 2017 [33]. These salts were chosen based on safety, availability, energy density and deliquescent relative humidity. Furthermore, $SrCl_2$ was added as additional salt based on screening and cyclic data of Mehrabadi and Farid in 2018 [14]. $CuCl_2$ was selected as additional model system.

First this work focuses on characterization of the matrix followed by a discussion of impregnating this matrix using saturated salt solutions. Second, the structures of the polymer-salt composite and deliquescence behavior are investigated. Third, cyclic tests are performed on a selected set of polymer-salt composites demonstrating their cyclic stability for

both hydration/dehydration and deliquescence/drying, while maintaining proper power output and structural integrity.

2. Materials and methods

2.1. Material fabrication

The polymer was synthesized according to the description of Kovačič et al. (2007) with some modifications such as stirrer speed and cyclohexane amount [30]. A detailed description of the polymer synthesis can be found in supplementary information S. 1.

Vacuum impregnation was performed by submerging the dried polymer into an already prepared salt solution for 90 min. Salt solutions were made by dissolving the desired amount of anhydrous salt (all obtained from Sigma Aldrich) in demineralized water. Five vacuum/pressurizing cycles were applied until no air bubbles were visible leaving the polymer matrix. This was done to enforce complete filling of the polymer pore space. After impregnation the samples were shortly treated with a burst of pressurized air to remove the excess of salt solution on the surface of the polymer. The polymer-salt composite was dried inside an oven at 130 °C for 4 h. After 3 h the weight was recorded and compared with the weight after 4 h to confirm complete drying.

The volumes of the starting empty polymer matrix and final dry composite were measured using a Mitutoyo digital caliper. Care was taken not to compress the composite during volume measurements. The volume increase from impregnation (swelling) $Q[\%]$ was calculated using

$$Q = \left(\frac{V_t}{V_e} - 1\right) \cdot 100\%. \quad [3]$$

Here $V_e[m^3]$ and $V_t[m^3]$ represent the empty volume of the polymer matrix and the total volume of the anhydrous polymer-salt composite, respectively.

Normal impregnation without vacuum was performed in a similar manner as vacuum impregnation without applying vacuum/pressurizing cycles.

2.2. pH measurements

Measurements of the solution pH was performed using a Metrohm 913 pH meter, equipped with a Unitrode Pt 1000 combined temperature and pH electrode. This way, the pH was determined with an accuracy of 0.01 in the temperature range of 20 to 21 °C. A three-point calibration was performed using Certipur buffer solutions from Merck.

2.3. Thermogravimetric analysis (TGA)

TGA on polymer-salt composites was performed on a Mettler Toledo TGA/DSC3 + to characterize the reaction kinetics and stability of the fabricated composites. The TGA setup is equipped with a home build humidifier generating different water vapor pressured by mixing a completely wet and completely dry nitrogen gas stream. This makes is possible to perform cyclic studies without removing the samples from the TGA device.

Polymer-K_2CO_3 and LiCl composites were subjected to isobaric water vapor pressures of 10 or 12 mbar and a nitrogen gas flow of 0.3 $L \cdot min^{-1}$. A single isobaric cycle consisted of the sample being subjected to 130 °C for 4 h to ensure a perfectly dry composite, followed by cooling to 30 °C, which is the maintained temperature until full conversion.

Relative humidity (RH) calibration was done by checking the deliquescence of various salts at 25 °C (LiCl, K_2CO_3, $MgCl_2$ and $Mg(NO_3)_2$). Temperature calibration was performed by checking the melting point of three metals (indium, zinc and lead).

2.4. Scanning electron microscopy (SEM)

SEM analysis was performed on a FEI Quanta 600 using 10 kV and low vacuum measurements to reduce charge accumulation on the sample. Prior to imaging, the samples containing anhydrous salt were cryogenically fractured. This is done by freezing the samples in liquid nitrogen. This procedure gave samples with a clear fracture plane to facilitate imaging of the internal structure of the composites.

2.5. Dynamic vapor sorption (DVS)

Water sorption isotherms were measured with DVS on a TA Q5000 SA. The temperature was kept isothermal at 25°C during the complete measurement. The relative humidity (RH) was set to zero for 6 h to equilibrate the sample and completely remove any residual water. Next, the RH was increased from 0% to 90% RH with incremental steps of 10%, and in 4% increments from 90% to 98%. Lowering of the RH was done in a reverse manner using the same incremental steps. Proceeding to the next RH increment was initiated when the weight change of the sample was less than 0.005% for 1 h or after a maximum of 6 h at a fixed RH.

2.6. Differential scanning calorimetry (DSC)

DSC measurements were conducted on a Mettler Toledo DSC822e with the desired heating/cooling rates under nitrogen atmosphere. The temperature was first increased to 105 °C and kept isothermal for 15 min to remove any water present. This was done to reveal possible transitions otherwise hidden by the effects connected to the removal of water. Next, the sample was cooled to 25 °C and kept isothermal for 10 min to equilibrate the sample.

3. Results and discussion

3.1. Characterization of the porous polymer matrix

Polymer characterization was performed using SEM and DVS. SEM was performed to investigate the polymer structure; DVS was performed to examine the water vapor sorption capabilities.

3.1.1. SEM characterization

After polymerization a highly porous polymer is obtained with a total porosity of 85 percent (determined by Micromeritics using a Micromeritics Gyopyc). In Fig. 1 two SEM images of the polymer cross section are shown with one SEM image of the outer surface. The polymer consists of hollow spheres interconnected by holes in the sphere wall, which is in line with the observations in the work of Kovačič [30]. DSC was used to determine the wash-out efficiency of Kolliphor P188 which was found to be 99.98%, therefore no surfactant is present in the SEM images.

The SEM images of the polymer cross sections show an interconnected network of spherical pores. The spheres result from the removal of the internal phase whereas the connections between spheres originate from spots where organic droplets were touching. In contrast to the internal structure, the outer surface layer consists of a dense, non-porous structure. To exclude any surface effects, the dense outer layers were removed by cutting of the sample.

From the SEM images pores in the range of micrometer size are visible. Nitrogen adsorption showed no presence of micropores and mesopores of which the details are given in supplementary information S. 2. Therefore no effects such as deliquescence lowering due to nano-confinement are expected [34]. The precise macropore structure could not be identified using mercury intrusion due to the compressibility of the matrix. Due to the open interconnected pore network maximum filling during impregnation is expected.

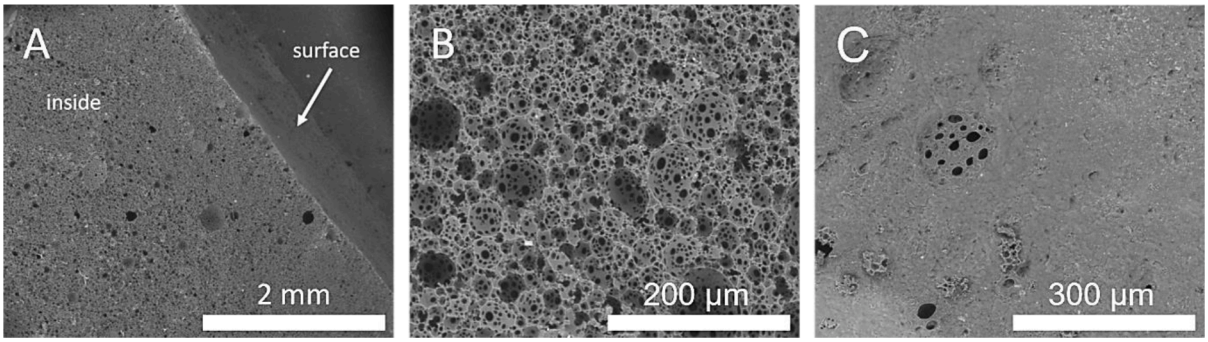

Fig. 1. SEM images of the polymer interior (cross-section, A and B) and surface (C).

3.1.2. Water sorption capability

Dynamic vapor sorption of the polymer matrix shows a gradual increase of moisture content with increasing relative humidity (RH) until around 60% RH, after which the increase accelerates (Fig. 2). At 25 °C and saturated water vapor conditions (100% RH) the polymer can absorb more than half of its weight in water. The upward concave shape corresponds to a Flory-Huggins isotherm similar to a type 3 Brunauer–Deming-Deming–Teller adsorption isotherm [35,36].

Due to the low amount of water uptake by the polymer matrix under the conditions for cyclic testing (~25% RH), the water uptake of the polymer can be neglected during cyclic testing of the polymer-salt composites. No significant hysteresis is observed indicating the absence of capillary condensation which could affect the impregnated salt under cycling.

When impregnating the porous polymer with liquid demineralized water, a water uptake of 7.8 ± 0.5 g/g and 5.8 ± 0.4 g/g were measured for vacuum impregnation and impregnating without vacuum respectively. The difference between the two impregnation methods indicates incomplete wetting of the polymer in the absence of vacuum. This most probably originates from air bubble being trapped inside the pores which are removed under vacuum. Therefore, vacuum impregnation is required to minimize the number of impregnation cycles required.

3.2. Impregnation of porous polymers with saturated salt solutions

The effect of multiple impregnation cycles on the evolution of salt content and salt density of the polymer-salt composite was investigated to determine the optimal number of impregnation cycles, assuming that repetitive impregnation is needed. The salt content and density for various polymer-salt composites as function of the number of impregnation cycles is displayed in Fig. 3. The salt content is given as the weight of the anhydrous salt m_s[g] divided by the weight of the empty polymer m_p[g]

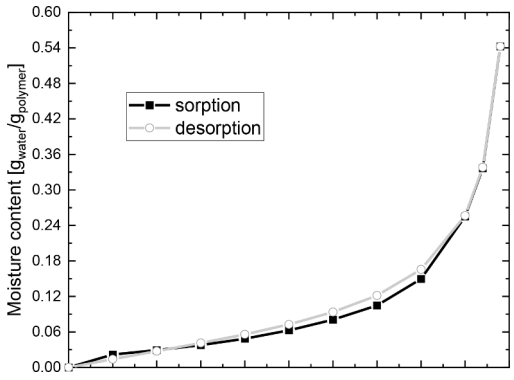

Fig. 2. DVS sorption/desorption measurement on a dry empty matrix.

$$\text{salt content} = \frac{m_s}{m_p}. \quad [4]$$

The overall salt density is given as the weight of the anhydrous salt divided by the total volume (described in section 2) of the polymer matrix filled with anhydrous salt after complete drying of the composite

$$\text{overall salt density} = \frac{m_s}{V_t}. \quad [5]$$

Note that in the case of $MgCl_2$ the salt should be present as the dihydrate after drying at 130 °C for four hours [37]. Higher drying temperatures were avoided to minimize HCl formation [33]. However, XRD analysis shows a mixture of dihydrate and tetrahydrate (denoted by di/tetra following $MgCl_2$), for de XRD diffractogram the reader is referred to the supplementary information S. 3.

When looking at the salt content LiCl, $MgCl_2$, $CuCl_2$, K_2CO_3 and $CaCl_2$ composites show an increase in salt content with increasing number of impregnation cycles. For $MgCl_2$ and $CaCl_2$ the last cycle seems to result in a lower salt content. However, the experimental errors overlap with the previous cycle.

When converting the salt content to the salt density it is visible that increasing the salt content is not always accompanied with an increase in salt density. This is due to swelling of the composited during impregnation. This mismatch may have implications for the optimal number of impregnation cycles, since more cycles does not necessarily contribute to higher salt densities.

For $CuCl_2$ only 2 impregnation cycles were possible due to the high acidity (pH of 0.90) of the saturated $CuCl_2$ solution. Combined with the high drying temperature, this most probably causes acid catalyzed hydrolysis of the ester and amide functionalities within the polymer matrix, after which the composite decomposes during the third impregnation cycle (Fig. 4). In the case of $SrCl_2$ no significant increase over the impregnation cycles is observed. From cycle 2 onwards, rapid formation of needle-shaped crystals is observed during impregnation most probably being the hexahydrate (Fig. 4) [38]. Crystallization of the salt lowers the concentration of ions in the solution penetrating the porous polymer which lowers the impregnation efficiency.

To elaborate on the mismatch between salt content and salt density the volume change of the dry impregnated composite compared to the empty polymer was measured as function of the impregnation cycles and volumetric salt content (Fig. 5). The volume change Q was calculate using equation 3 and the volumetric salt content per pore volume α was calculated as

$$\alpha = \frac{m_s \rho_p (1-n)}{m_p \rho_s n}. \quad [6]$$

Where ρ_s[g·cm^{-3}] and ρ_p[g·cm^{-3}] represent the anhydrous salt crystal and polymer density. Since for $MgCl_2$ a mixture of dihydrate and tetrahydrate exist the average density (1.77 g·cm^{-3}) of the dihydrate and tetrahydrate is used. The polymer matrix density was found to be 1.1 ± 0.1g·cm^{-3} (based on sample weight, volume, and porosity) and the

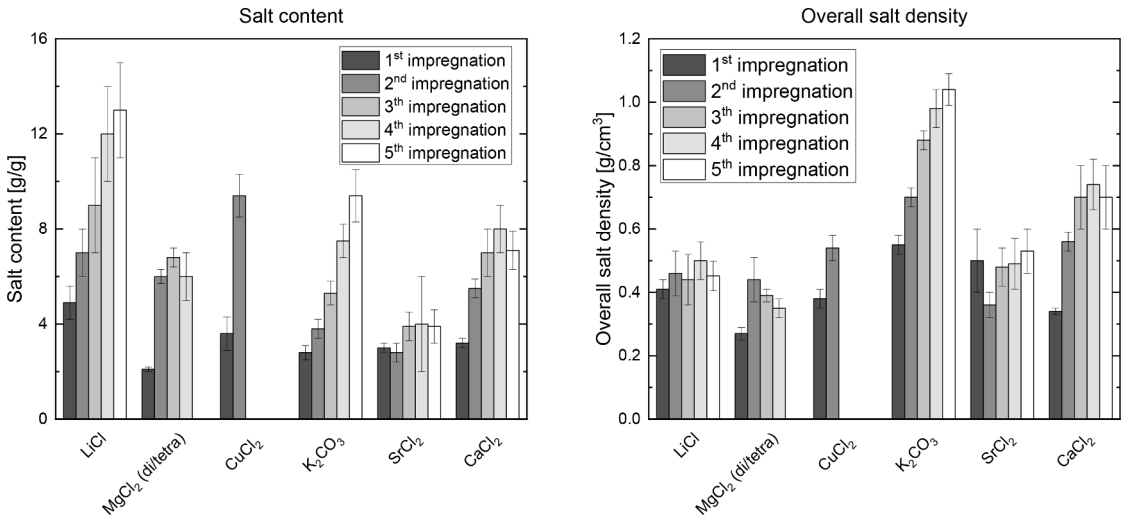

Fig. 3. Salt content in g/g (left) and salt density in g/cm^3 (right) for various polymer-salt composites as a function of the number of impregnation cycles. Drying was done at 130 °C for 4 h. Errors are calculated using a sample size of 3.

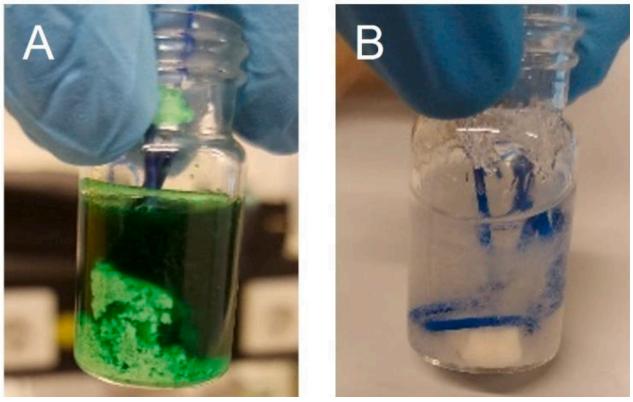

Fig. 4. Degradation during the third impregnation for a polymer-$CuCl_2$ composite (A) and crystal formation (white particles) during the second impregnation for a polymer-$SrCl_2$ composite (B). The dark blue part is a small weight to keep the polymer matrix submerged in the solution.

porosity $n[-]$ is 0.85. The used densities to calculate the volumetric salt content per pore volume are given in Table 2.

Impregnation with different salts shows different swelling behavior as function of the impregnation cycles (Fig. 5). For LiCl (dark grey circles), $MgCl_2$ (grey upward triangles) and $CuCl_2$ (light grey downward triangles) a strong increase in volume is observed with every cycle, whereas for K_2CO_3 (orange diamonds) a more gradual increase is observed. In the case of $SrCl_2$ (blue leftward triangles) and $CaCl_2$ (green

Table 2
Crystal densities for various salts obtained from literature. All densities are anhydrous densities except for $MgCl_2$.

salt	Density ρ_s[g·cm^{-3}]	Reference
LiCl	2.09	[39]
$MgCl_2$ (dihydrate)	1.90 (at 369 K)	[40]
$MgCl_2$ (tetrahydrate)	1.64 (at 358 K)	[41]
$CuCl_2$	3.44	[42]
K_2CO_3	2.43	[43]
$SrCl_2$	3.10	[44]
$CaCl_2$	2.19	[45]

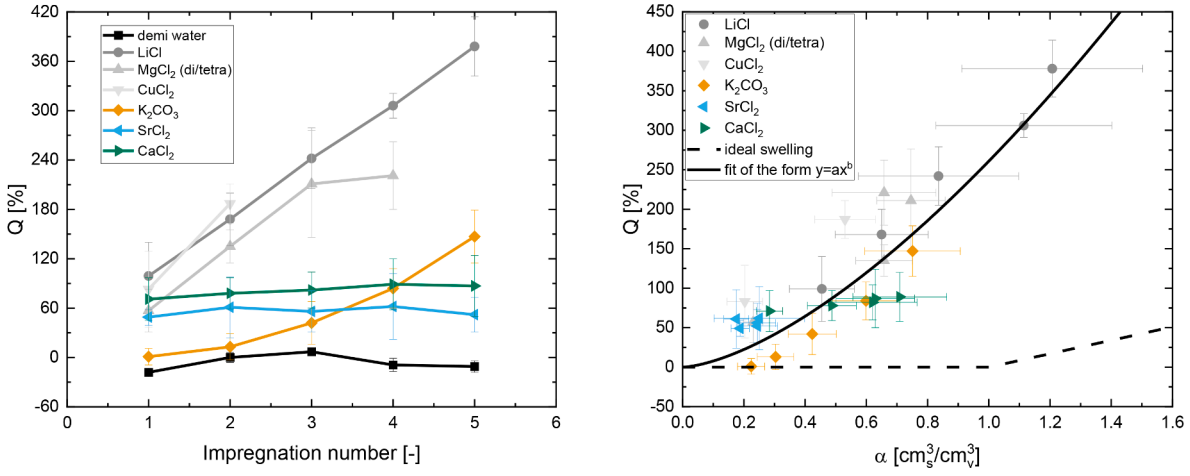

Fig. 5. Volume change of the dried composite compared to the original empty polymer matrix for different salt versus the number of impregnation cycles (left) and volumetric salt content per pore volume (right). The black line represents a fit of the form $y = ax^b$. The subscript s represents the salt and v represents the void space. Errors are calculated using a sample size of 3.

rightward triangles) almost no change is observed after the first cycle. As a reference, multiple impregnations using demineralized (demi) water (black squares) were conducted from which it is clearly visible that the polymer prefers to return to its initial shape after drying. As a result, the salt causes the increase in volume.

Fig. 5 shows that the overall swelling increases with the volumetric salt content per pore volume and is always above the ideal swelling line. The ideal swelling line is the expected volume increase when all salt is filling the available pore space. In the ideal case up until $\alpha = 1$ no swelling is expected, whereas after $\alpha = 1$ the swelling is expected to increase linearly with α. The volume increase is already occurring before all pore space is filled as seen in Fig. 5.

Several explanations can be given. First, the polymer swells when placed into water and salt solutions. Upon drying the polymer matrix wants to revert to its original shape. This is supported by the fact that the polymer impregnated with pure water reverts to its original shape upon drying. When crystallization of salt occurs, the matrix movement is limited, and the original shape cannot be achieved. Second, the SEM images discussed in detail in section 3 show that the distribution of salt is not always homogeneous and clustering of particles and crust formation at the edges occurs which can exert expanding forces on the polymer matrix.

Due to the increase in composite volume, the overall salt density in the composite will decrease once the volumetric salt content becomes too high.

A top three selection in salts emerges for further cyclic testing which are: LiCl, K_2CO_3 and $CaCl_2$. $CuCl_2$ caused degradation of the polymer (Fig. 4) and the needle shaped crystals formed when using $SrCl_2$ results in damage of the polymer as can be seen in the SEM image in Fig. 6. In the case of $MgCl_2$ incomplete dehydration occurred leading to a mixture of hydration states. At higher dehydration temperatures $MgCl_2$ is prone to form undesired HCl.

3.3. The structure of salt impregnated polymer composites

Next, the structure of the impregnated composites is investigated to identify the location and structure of the salt hydrate in the matrix, since this can have implication on the stability. The composites investigated were a K_2CO_3, $CaCl_2$ and LiCl impregnated polymer. The K_2CO_3 and $CaCl_2$ composites were impregnated 5 times to obtain a higher overall salt density. The LiCl composites was impregnated only once since multiple impregnations do not significantly increase the overall salt density (Fig. 3).

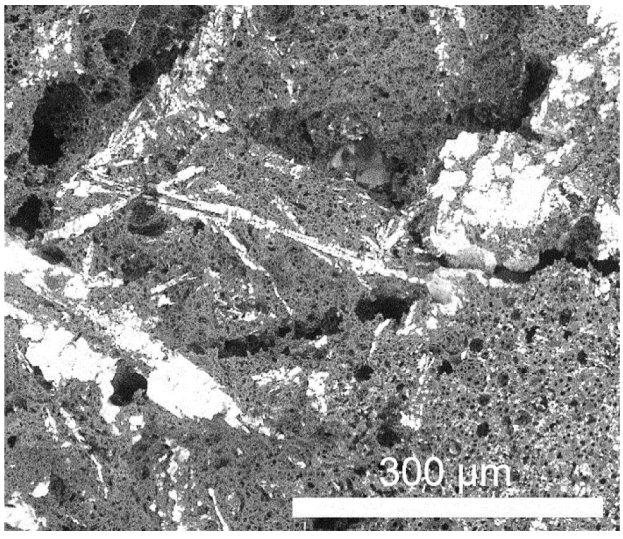

Fig. 6. SEM image of a polymer-$SrCl_2$ composite after 5 impregnation cycles. The SEM image (cross-section) shows damage (cracks) done to the polymer by the needle shaped crystals.

Fig. 7 shows a K_2CO_3-polymer composite after 5 impregnation cycles. The SEM images show K_2CO_3 grains distributed within the polymer matrix. The salt grains have a diameter of around 20 µm that are embedded within the pore space. The inside of the individual salt grains consists of porous structure as well. SEM images of salt grains recrystallized from a saturated solution at 130 °C showing similar porous structures can be found in the supplementary information S. 4.

In the case of the $CaCl_2$ filled composite in Fig. 8, the situation is different compared to the K_2CO_3 filled composite. The $CaCl_2$ filled composite shows an enrinched layer near the outer surface of the composite particle. The salt grains found inside the matrix are much smaller in size compared to the grains in K_2CO_3 filled matrix.

Lastly, the LiCl filled composite was imaged (Fig. 9). As with $CaCl_2$, an enriched boundary layer is found with a width of about 400 µm. The diameter of the salt grains found inside the matrix is smaller than the size in K_2CO_3 filled polymer.

The difference in structure between the K_2CO_3 and $CaCl_2$ or LiCl composite can be explained by considering the wettability of the polymer by the salt solution. When placing a droplet of saturated LiCl or $CaCl_2$ solution on top of the polymer, the droplet spreads over the surface indicating proper wettability. When doing the same for a K_2CO_3 solution the droplet remains on top of the polymer surface indicating poor wettability (Fig. 10).

The drying behavior of wetting and non-wetting solutions are distinctly different. In porous media, wetting solutions tend to dry homogeneously, whereas in the case on non-wetting solutions an inward drying front exist [46]. In the case of a wetting salt solution, drying results in the movement of ions toward the drying surface. Since the ions cannot leave the material, crystallization occurs at the drying surface [47]. This explains the dense salt layer inside the LiCl and $CaCl_2$ composites since both solutions are wetting the polymer. Since the K_2CO_3 solution is a non-wetting solution, and inward drying front occurs resulting in uniform crystallization of salt throughout the matrix.

3.4. Feasibility of the deliquescence transition

The deliquescence of the impregnated polymer structures was investigated for two reasons. First, to examine whether the deliquescence transition can be used to store heat and second, whether the composite can be exposed to deliquescent condition without leakage of the solution.

Different salt impregnated composites are placed into a chamber for one week containing their respective saturated salt solution (see Fig. 11). Next to LiCl, $CaCl_2$ and K_2CO_3 different other salts ($MgCl_2$, $CuCl_2$, $SrCl_2$, $NaNO_3$ and Na_2CO_3) were tested to investigate whether a general trend exists. A single impregnation cycle was performed to ensure that the matrix should be able to easily hold the complete salt solution volume within its pore system.

Obviously, the non-wetting carbonate solutions leak out of the polymer upon deliquescence, whereas the other wetting salt composites are stable showing no leakage. The only exception is $SrCl_2$. For the non-wetting carbonate solution some deliquescence stability is provided in the sense that the deliquescence and leakage of solution is slowed down. Leakage of the solution occurred after several days whereas mm-sized particles or powder can undergo complete deliquescence in hours to minutes.

3.5. Cyclic stability of salt-polymer composites

The kinetic and structural cyclic stability of the polymer composites was evaluated using TGA. Composites containing K_2CO_3, $CaCl_2$ and LiCl were investigated. For the K_2CO_3 composite the anhydrous to sesquihydrate transition is investigated, whereas in $CaCl_2$ the anhydrous to dihydrate transition was assessed. For LiCl the deliquescence transition was investigated due to the low deliquescence relative humidity (DRH)

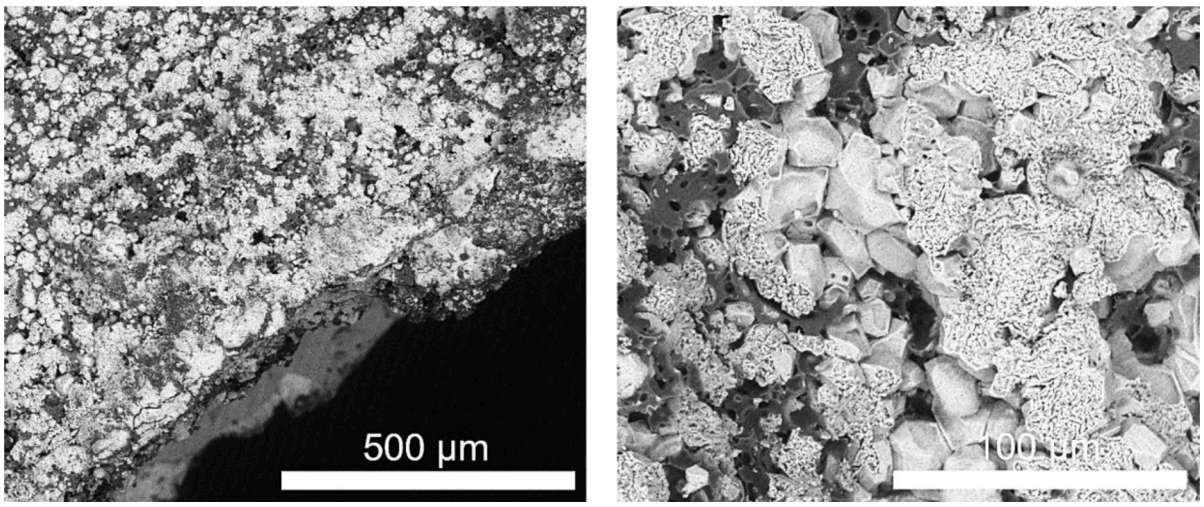

Fig. 7. SEM images (cross-section) of the K_2CO_3 filled polymer matrix after 5 impregnation cycles.

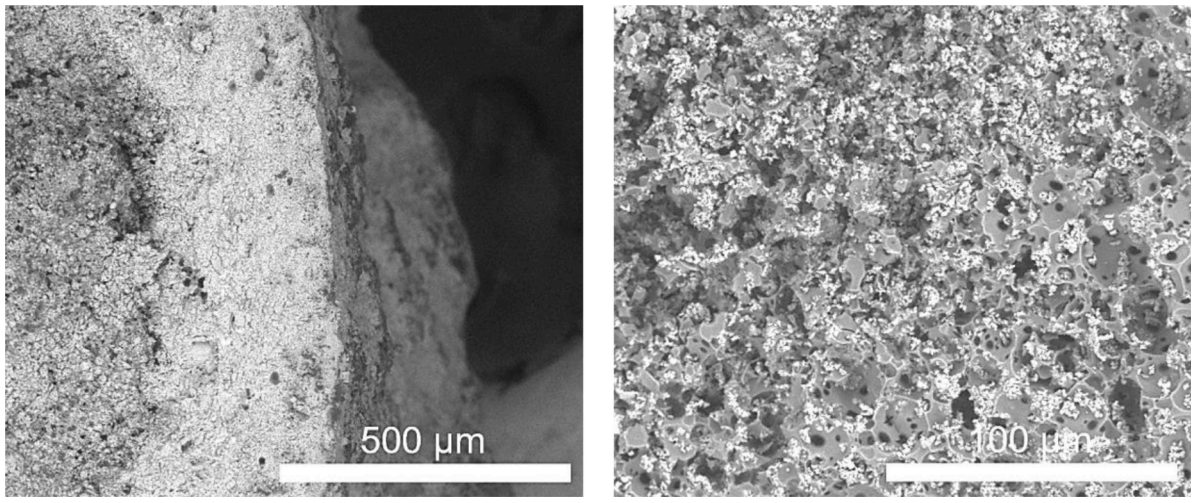

Fig. 8. SEM images (cross-section) of the $CaCl_2$ filled polymer matrix after 5 impregnation cycles. An enriched salt layer of around 300 μm is present near the composite surface.

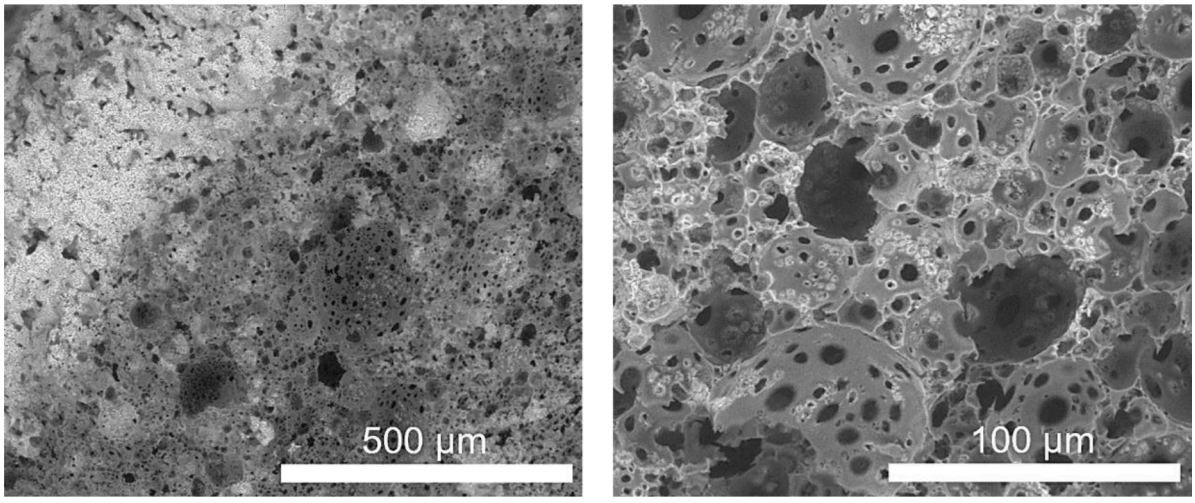

Fig. 9. SEM images (cross-section) of the LiCl filled polymer matrix after 1 impregnation cycle. An enriched salt layer of around 400 μm is present near the composite surface.

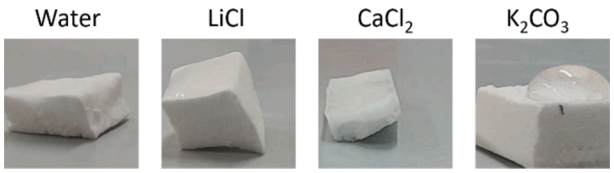

Fig. 10. Wettability of the polymer matrix by the saturated solutions.

of LiCl which is lower than the 12 mbar of water vapor identified as a typical operating condition [33].

3.5.1. Potassium carbonate

A potassium carbonate-polymer composite containing 10 g/g of K_2CO_3 was cycled under isobaric conditions (12 mbar of water vapor) by varying the temperature (30 °C for hydration until full conversion and 130 °C for dehydration for four hours). These conditions were chosen to make sure that cycling occurred outside of the metastable zone, where nucleation limits the reaction rate as was identified by Sögütoglu et. al. (2019) [2]. In addition, these conditions did not lead to deliquescence according to the phase diagram [2]. The dehydration/hydration cyclic curves and power output per kg of salt are given in Fig. 12. The first hydration event is considered as an activation cycle due to its very slow kinetics. Cycle 1 is the first cycle after the activation cycle.

An activation cycle is necessary to break up the salt grains blocking the pores in which they have crystalized, this activation cycle is given as the insert in Fig. 12. Most of the activation hydration curve shows a linear dependence of the loading vs. time, indicative for a situation in which the hydration kinetics are determined by the permeability through these salt grains instead of diffusion throughout the composite pore system. For the first cycle (cycle 1) after the activation cycle, the linearity disappeared, and the kinetics accelerate with increasing number of cycles. After approximately cycle 30, stabilization seems to occur and no significant increase in kinetics over the cycles is observed.

The hydration kinetics improves over cycles since diffusion is improved due to fragmentation of these crystals over multiple cycles [5]. This fragmentation is clearly visible when comparing Fig. 13A with Fig. 7. After 5 cycles the dense particles found in Fig. 7 become porous (Fig. 13).

The composite performance can be evaluated using the instantaneous power output per kilogram of anhydrous salt $P[\mathrm{W{\cdot}kg^{-1}}]$ defined as

$$P = \frac{dN}{dt}\frac{\Delta H}{m_s}. \quad [7]$$

Here $N[\mathrm{mol}]$ represents the moles of reacted water, $t[\mathrm{s}]$ is the time and $\Delta H[\mathrm{J{\cdot}mol^{-1}}]$ the enthalpy of reaction, which is calculated from literature to be 63.6 $\mathrm{kJ{\cdot}mol^{-1}}$ [48]. The water vapor uptake rate (dN/dt) in equation 7 is calculated from differentiating the loading versus time curve from which the instantaneous power output is then calculated.

The instantaneous power output for all cycles has a peak after the first few milligrams of water uptake after which the power decreases with water uptake. This behavior resembles a diffusion limited system for which the initial kinetics is high and quickly decreases once a reaction front is established [26].In the case of a nucleation limited system, the reaction at the salt grains would be rate determining, and the power/uptake curve would have a parabolic shape with a higher sustained power output [49].

Next to the kinetic study, visual inspection showed the structural evaluation of the K_2CO_3-polymer composite for 50 cycles (Fig. 14). The composite retains its original shape without significant degradation. Only at higher cycles (>30) swelling of the composite occurs. This swelling is caused by salt creeping out of the polymer matrix and

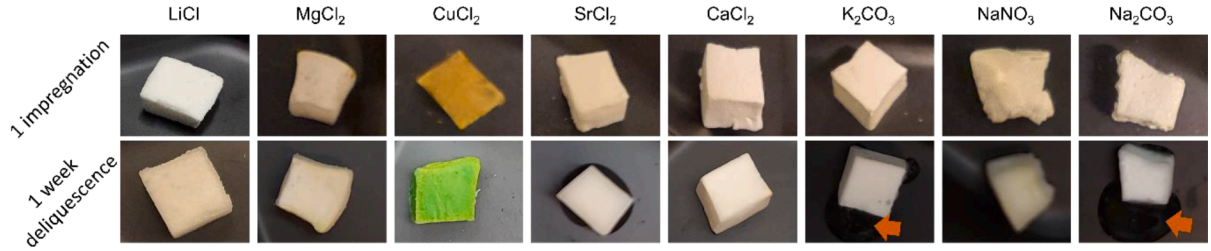

Fig. 11. Images of different salt-polymer composites before deliquescence and after 1 week of deliquescence in their respective saturated salt solution. In the case of $CuCl_2$ the anhydrous salt is brown whereas the deliquescent salt exhibits a green color. The red arrow indicates leaking of the salt solution.

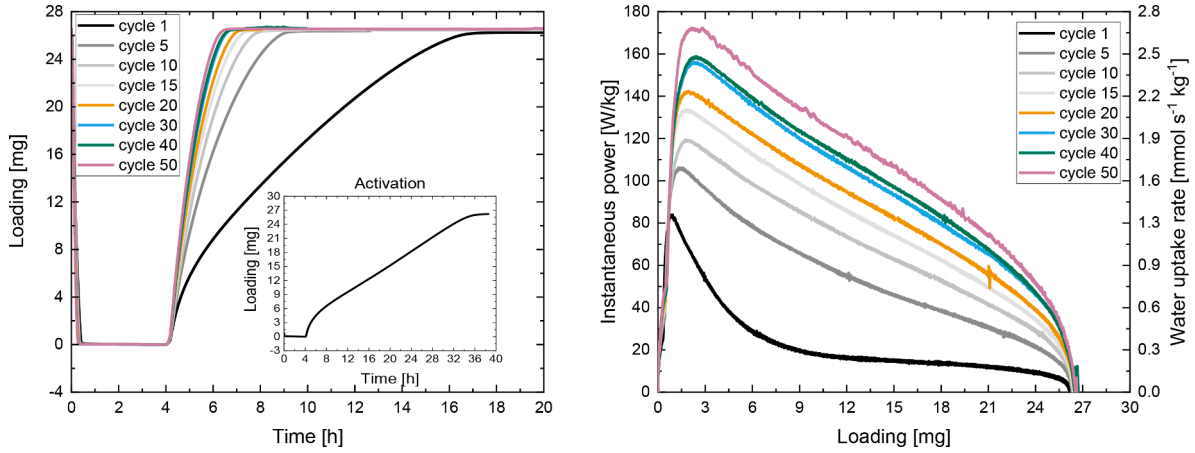

Fig. 12. Dehydration/hydration cyclic curves for the activation cycle and real cyclic tests (left) and instantaneous power output per kg of dry salt (right). Cycling was done under isobaric conditions (12 mbar of water vapor) by varying the temperature (30 °C for hydration until full conversion and 130 °C for dehydration for four hours). The maximum loading was equal to the expected loading based on the 0–1.5 transition. Transformation from the left to the right graph was done by differentiating the left graph and using equation 7.

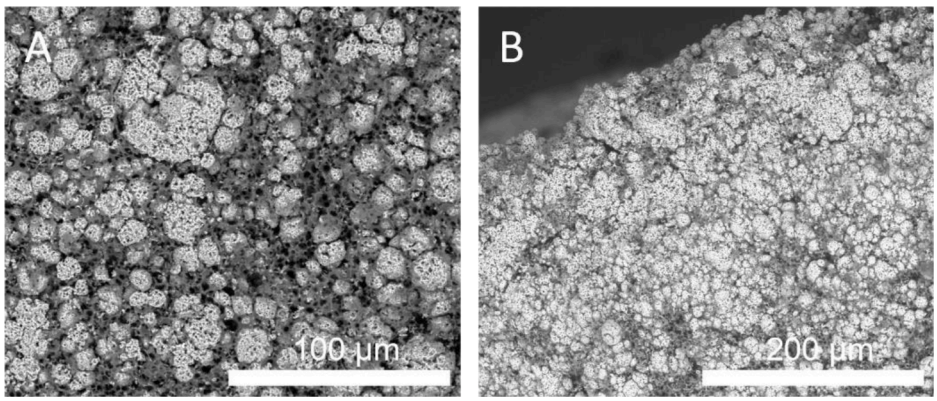

Fig. 13. Cross-section SEM images of a K_2CO_3 impregnated matrix cycled 5 times. Images were taken inside the composite (A) and near the composite surface (B).

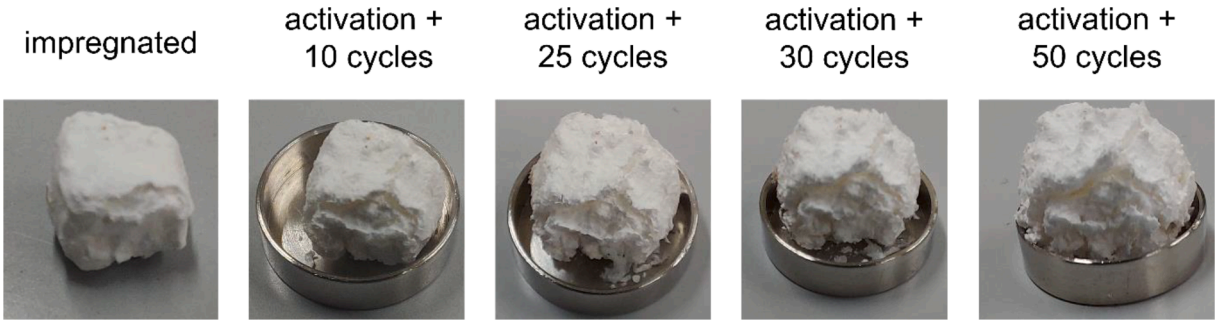

Fig. 14. Visual inspection of the K_2CO_3-polymer composite before and after cycling. Note that the first picture has salt in the anhydrous form whereas the other pictures contain the salt in hydrous form.

crystalizing on the composite surface. Since the hydration proceeds via a wetting layer, consisting of a non-wetting salt solution, over cycles the salt will creep out of the system similar to a deliquescent system (Fig. 11) [2]. During every hydration, the wetting layer will migrate a short distance towards the composite surface where the newly formed hydrate crystalizes. Every cycle this process repeats resulting in the salt crystal migrating over several millimeters after a given amount of hydration/dehydration cycles. The migration of salt towards the composite outer surface can also be seen when comparing Fig. 13B with Fig. 7. The salt density near the composite surface is increasing after 5 cycles.

The composite after 50 cycles was still mechanically stable. Placing the cycled composite in water dissolving the salt yields back the original size of the polymer matrix.

3.5.2. *Calcium chloride*

Next, a calcium chloride-polymer composite containing 7 g/g of $CaCl_2$ was cycled under isobaric conditions (10 mbar of water vapor) by varying the temperature (40 °C for hydration until full conversion and 130 °C for dehydration for four hours). These conditions were chosen since they should produce the dihydrate [50]. The uptake versus time and power output/water vapor uptake rate a given in Fig. 15.

The hydration curves follow the same trend as in the case of the

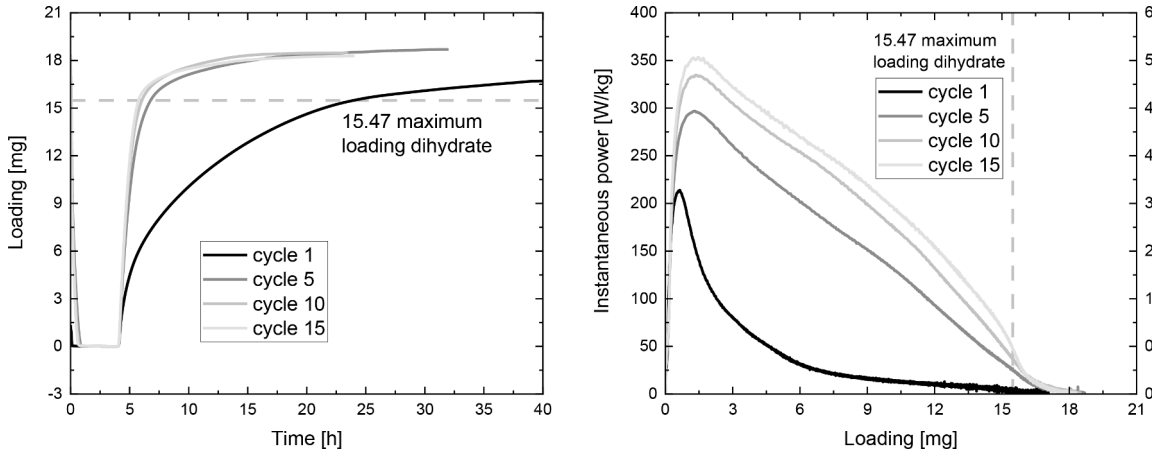

Fig. 15. Dehydration/hydration cyclic curves for the cyclic tests (left) and instantaneous power output per kg of anhydrous salt (right). Cycling was done under isobaric conditions (10 mbar of water vapor) by varying the temperature (40 °C for hydration until full conversion and 130 °C for dehydration for four hours). The dashed lines at an uptake of 15.47 mg indicates the theoretical uptake at which all salt has been converted into the dihydrate. Transformation from the left to the right graph was done by differentiating the left graph and using equation 7.

K_2CO_3 polymer composite. The first cycle is slow after which kinetics increase to stabilize after 10 cycles. Although the conditions of hydration are chosen to produce the dihydrate, additional uptake is observed. This additional uptake could be caused by local formation of the tetrahydrate (see supplementary information S. 5. for XRD spectra). No detailed phase diagrams including possible metastable zones are reported yet, but no induction times are observed. Therefore, it is valid to believe that the chosen conditions are outside the metastable zone.

The power output is calculated using equation 7 with ΔH equal to 61.8 kJ·mol^{-1} [48]. The first hydration cycle shows similar diffusion limitations as the first cycle for the K_2CO_3 polymer composite. The subsequent cycles, the power output curves start to resemble hydration kinetics which are less limited by diffusion as was also observed for the K_2CO_3 polymer composite when kinetic stabilization starts to occur. A major difference with the K_2CO_3 composite is that there is no linearity in the first cycle and therefore an activation cycle is absent in the $CaCl_2$ composite. This is most probably due to the enriched salt layer near the surface behaving as a porous compacted mm-sized particle.

Additionally, visual inspection was performed (Fig. 16). Up to ten cycles no change in composite structure is observed. However, after 15 cycles a salt shell has formed around the outside of the composite. We hypothesize that this shell originates from the dense salt layer near the surface, as seen on the SEM images in Fig. 8. Upon hydration the salt at the surface most probably is expanding outwards resulting in this salt shell. Contrary to the swollen K_2CO_3 polymer composite, the salt shell around the $CaCl_2$ polymer composite is very brittle and crumbles when touched. Therefore, cyclic experiments were stopped since the efflorescing salt layer was disintegrating after 15 cycles. Dissolution of the salt after 15 cycles yields back the original empty matrix before impregnation.

3.5.3. Lithium chloride

Lastly a lithium chloride-polymer composite containing 4 g/g of LiCl was cycled under isobaric conditions (10 mbar of water vapor) by varying the temperature (30 °C for hydration until full conversion and 130 °C for dehydration for four hours). These conditions are far above the deliquescence water vapor pressure (~4.5 mbar at 30 °C) and were chosen to demonstrate that the matrix can accommodate additional water uptake (due to swelling). Otherwise, this would leak out of a fully saturated rigid matrix. The cyclic drying/deliquescence and rate curves are given in Fig. 17.

Fig. 17 shows that a full kinetic cycle can be done within 16 h. The deliquescence kinetics are stable over all cycles, which is underlined by the water uptake rate curves. In the case of drying the deliquescent composite a longer drying time is required over the cycles. Until all salt has formed a saturated solution, the water uptake rate drops only slightly, whereas in the region of dilution the rate decreases more steeply. Similar deliquescence kinetics for all cycles were expected, since upon drying the same starting (dry) material is produced in every cycle.

To evaluate the performance, the water uptake rate was converted into a power output (Fig. 18). At a water uptake of 23.58 mg all salt theoretically should have gone into deliquescence.

It is assumed that, first, all salt crystals go into deliquescence to form a saturated solution and, second, the saturated solution is further diluted [4,51]. As a result of this, the enthalpy ΔH (from equation 7) consists of two parts, which differ whether a saturated solution has been formed or not. Before complete dissolution of all crystals ΔH consist of the condensation enthalpy of water ΔH_c and solvation enthalpy ΔH_s of LiCl into a saturated solution [3]. Used values for ΔH_c and ΔH_s are 46 kJ·mol^{-1} [52] and 37 kJ·mol^{-1} [53], respectively. When all crystals have dissolved, the enthalpy of solution is replaced by the enthalpy of dilution ΔH_d and ΔH_d has the value of 5.5 kJ·mol^{-1} [52].

When performing visual inspection, it is found that the composite is completely stable for a minimum of 30 cycles (Fig. 19). No swelling or geometrical changes were observed over cycling. However, visual inspection after cycle 40 showed degradation of the composite. Retrieval of the polymer matrix was not possible as the composite turned into a slurry-like structure. This is most probably due to hydrolysis of the ester and amide bonds within the concentrated salt solution during drying of the composite at elevated temperatures. Catalytic hydrolysis of esters [54] and amides [55] by Li^+ ions under various conditions is also observed in literature. Therefore, it is believed that lithium ions are responsible for the polymer degradation.

The hydrolysis of the polymer matrix could also be responsible for the changing drying kinetics over cycles (Fig. 17), since drying and crystallization of the LiCl is dependent on the precise environment. However, the hydrolysis of the matrix does not result in any volatile products since no additional weight loss is observed during drying.

3.6. Implications for thermochemical heat storage

Due to the different wetting behavior of salt solutions on the polymer matrix, three feasible combinations of salt, polymer and discharge conditions are possible for cyclic testing. In the case of a salt forming a nonwetting salt solution (K_2CO_3), a uniform distribution of salt is found within the polymer matrix, whereas wetting salt solutions ($CaCl_2$ and LiCl) form an enriched salt layer at the composite surface.

Apart from the salt distribution, the wetting behavior dictates which discharge conditions are feasible. In the case of non-wetting salts only the hydration transition is feasible since deliquescence of the salt results in leakage of the deliquescent solution. However, since leakage of the deliquescent solution takes several days handling and transport of the composite under deliquescent could be possible. For salts forming wetting solutions both the hydration and deliquescence cycles can be used.

When comparing cyclic hydration/dehydration of the K_2CO_3-polymer composites (non-wetting and homogenously distributed) with the

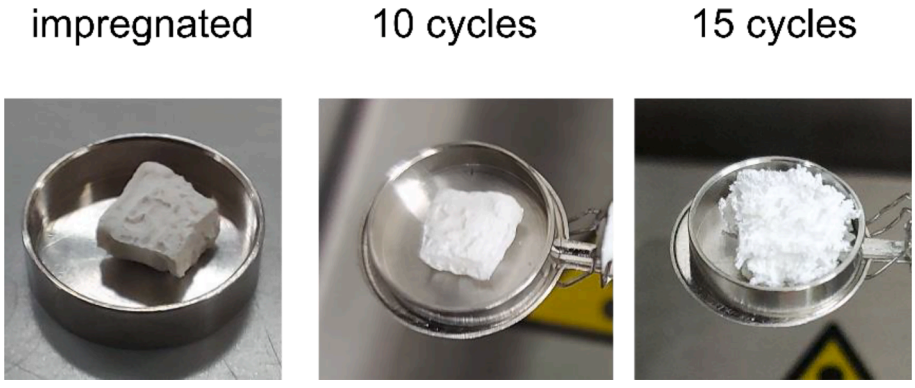

Fig. 16. Visual inspection of the $CaCl_2$-polymer composite before and after cycling. Note that the first picture has salt in the anhydrous form, whereas the other pictures contain the salt in hydrous form.

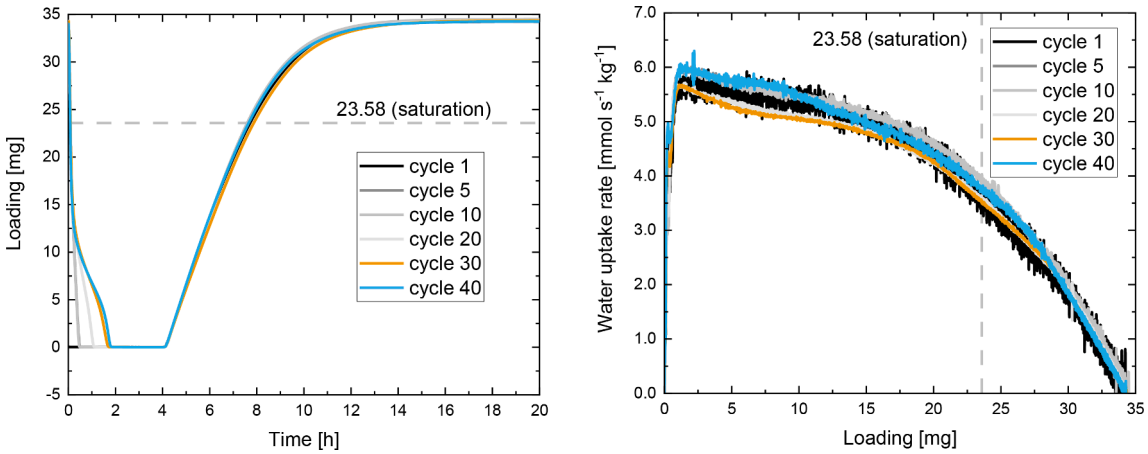

Fig. 17. Drying/deliquescence cyclic curves (left) and water vapor uptake rate per kg of dry salt (right). Cycling was done under isobaric conditions (10 mbar of water vapor) by varying the temperature (30 °C for hydration until full conversion and 130 °C for dehydration for four hours). The dashed lines at an uptake of 23.58 mg indicates the theoretical uptake at which all salt has gone into deliquescence and a saturated solution inside the matrix is formed. Transformation from the left to the right graph was done by differentiating the left graph.

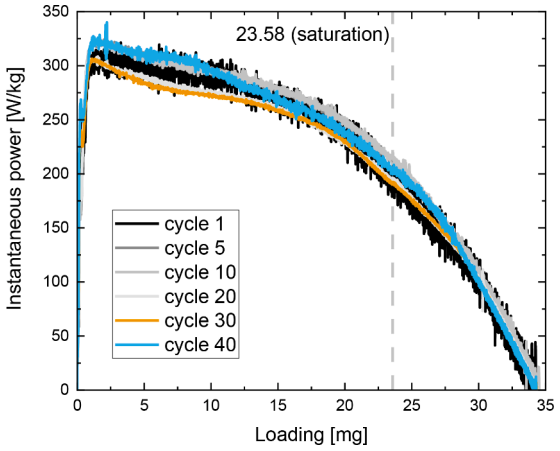

Fig. 18. Instantaneous power output per kg of dry salt. Cycling was done under isobaric conditions (10 mbar of water vapor) by varying the temperature (30 °C for hydration until full conversion and 130 °C for dehydration for four hours).

$CaCl_2$-polymer composite (wetting and enriched salt layer near the composite surface) several observations can be made. The non-wetting salt migrates towards the composite surface after multiple (>30) cycles, whereas the wetting salt protrudes from the composite surface after a lesser number of cycles (15). This results in the fact that composites made with non-wetting salts swell at higher cycles and, that most likely, their cyclic lifetime is determined by the stability of the protruding salt layer. In the case of wetting salts, a different fabrication method to ensure a homogeneous distribution of salt inside the matrix is recommended to prevent salt protrusion. Available options include freeze drying or low temperature drying.

For wetting salt solutions, the main advantage is the use of the deliquescence transition, since this is accompanied by higher energy densities compared to hydration only. Another key observation is that the LiCl composite does not swell with increasing cycles. However, the polymer-salt combination must be tuned accordingly to prevent degradation in the electrolyte (Salt) solution as observed with the LiCl-polymer composites after 40 cycles.

Donkers et al. selected various promising salts based on the criteria that a TCM should be able to reach 65 °C and 40 °C for domestic hot water production and space heating, respectively, using water vapor pressures of 12 mbar [33]. The composites studied in this work can deliver temperatures above 40 °C at 12 mbar (or less) of water vapor pressures, whereas none is suitable for hot water production (≥ 65 °C).

For LiCl-polymer composites a temperature of 45 °C can be delivered at 10 mbar, increasing the vapor pressure to 12 mbar only increases the output temperature to 48 °C [2]. For a K_2CO_3 composite at 12 mbar, an output temperature of 60 °C can be reached [2]. Lastly, for a $CaCl_2$ composite 58 °C can be reached using 10 mbar whereas 12 mbar increases the output temperature to 61 °C [50].

Next to the output temperature, composite performance (power output) and energy density are important. The hydration power output for the K_2CO_3 and $CaCl_2$ composites in the first cycles is already higher compared to mm-sized pure K_2CO_3 particles in which the reaction rate and power output are low [26]. During cycling the power output increases up to a few hundred Watt per kilogram and is sustained over higher conversion.

Compared to powder samples, the composite samples are slower

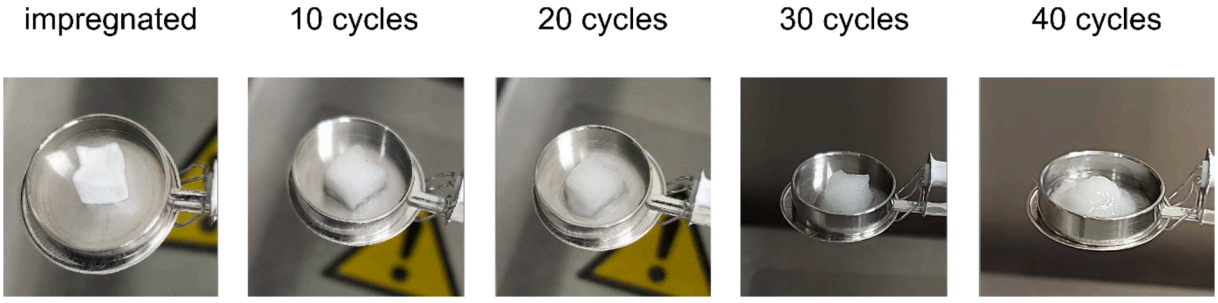

Fig. 19. Visual inspection of the LiCl-polymer composite before and after cycling. Note that the first picture has salt in the anhydrous form whereas the other pictures contain the salt in deliquescent form.

because diffusion limitations exist within the polymer matrix. For the K_2CO_3 composite the peak power output after 50 cycles is similar tot the first cycle of the powder. This indicates that the composite is become more reaction limited with cycling. In the case of the $CaCl_2$ composites the peak power output of the powder is not reached within the current cycles (Table 3).

In the case of deliquescent cycling (LiCl composites) the maximum power output is already obtained in the first cycle and does not change over cycling. In addition to mechanical stability also kinetic stability is obtained.

In Table 4 the material storage density [$GJ \cdot m^{-3}$] (*MSD*) of different systems are given. The MSD is defined as the energy density of a single particle or composite particle

$$MSD = \frac{\sum(n_i \cdot \Delta H_i)}{V_t}. \quad [8]$$

Here n_i[mol] and ΔH_i[$GJ \cdot mol^{-1}$] represent the number of moles and the associated enthalpy respectively. For hydration this is simply the total number of reacted moles of water multiplied by the hydration enthalpy. For deliquescence the summation consists of the total moles of water condensing and dissolving the salt and a second term consisting of the total moles of water condensing and diluting the saturated solution. Again it is assumed that, first, all salt crystals go into deliquescence to form a saturated solution and, second, the saturated solution is further diluted [4,51]. The composites of this work are compared to recent literature using the same salt hydrates.

Energy density of the composites from this work are higher compared to recent literature. This is due to the multiple impregnation steps and high pore volume of the matrix. For $CaCl_2$ literature examples could only be found for the 0 to 6 transition, but when utilizing the 0 to 6 transition for the $CaCl_2$-polymer composite from this work higher energy densities are expected. The MSD of the K_2CO_3 composites is lower compared to the mm-sized pure K_2CO_3 particles since the non-stabilized particles consist of the pure salt with a low porosity. However, the stabilized composites compensate this loss in MSD with high power output. Similar observations are expected for other salts.

When comparing the three tested composites the composite containing LiCl is superior to the other two salts. The LiCl composite has the highest energy density and power output, the best mechanical stability (no swelling), kinetic stability over cycling and deliquescent stability. Therefore, the most promising method of stabilization and discharge condition is using a wetting salt and deliquescence as discharge condition.

When using prices found on Sigma Aldrich for hydroxyethyl methacrylate (HEMA) and *N*,*N*′- methylene bisacrylamide (MBAA) a price of roughly 500 euros per kilogram of empty matrix can be calculated. Using this price and the salt content from Fig. 3 approximately 2500 to 5000 kg of salt can be stabilized with this amount of polymer. When using potassium carbonate from Sigma Aldrich as an example this results in 165,000 to 330,000 euros worth of salt, showing that the price of the pure matrix is insignificant compared to the price of salt. Actual fabrication and processing steps are not included in the calculation.

Table 3
Peak power output for the stabilized materials in this work and powder samples (K_2CO_3 and $CaCl_2$) under similar conditions. TGA of the powder samples can be found in supplementary information S. 6.

Method	Peak power [W ·kg]	Hydration transition	Discharge conditions	Reference
K_2CO_3-polymer	Cycle 1: 82 Cycle 50: 172	0–1.5	12 mbar, 30 °C	This work
K_2CO_3 powder	Cycle 1: 162	0–1.5	12 mbar, 30 °C	This work
$CaCl_2$-polymer	Cycle 1: 214 Cycle 15: 353	0–2	10 mbar, 40 °C	This work
$CaCl_2$-powder	Cycle 1: 1038	0–2	10 mbar, 40 °C	This work
LiCl-polymer	325	deliquescence	10 mbar, 30 °C	This work

Table 4
Material storage densities (MDS) for the stabilized materials in this work and other literature examples. The mm sized K_2CO_3 particles are not stabilized.

Method	MSD [G $J \cdot m^{-3}$]	Hydration transition	Discharge conditions	Reference
K_2CO_3-polymer	0.5	0–1.5	12 mbar, 30 °C	This work
K_2CO_3 powder	1.3	0–1.5	Theoretical max.	[33]
K_2CO_3-vermiculite	0.3	0–1.5	23 mbar, 40 °C	[12]
mm sized K_2CO_3 particles	1.0–1.2	0–1.5	7.7 mbar, 20 °C	[26]
$CaCl_2$-polymer	0.8	0–2	10 mbar, 40 °C	This work
$CaCl_2$-powder	1.5	0–2	Theoretical max.	[33]
$CaCl_2$-hollow silica	0.9	0–6	10 mbar, 45 °C	[7]
LiCl-polymer	2.4	deliquescence	10 mbar, 30 °C	This work
LiCl- hollow silica	0.5	deliquescence	15 mbar, 45 °C	[7]

A final remark focusing on the thermal conductivity of polymers related to the application must be made. Salt hydrates and their composites can be used in two different systems, open and closed. In closed systems the reactor is operated under pure water vapor conditions with higher power output compared to open systems. However, open systems are less complex. Michel et. al. (2014) identified the main limitations for open and closed systems. The authors showed that for open systems mass transfer is the main limitation whereas in closed systems heat transfer is [56]. Therefore, the presented composite is suitable for application in open systems. For application in closed system the thermal conductivity must be enhanced which is possible through addition of fillers [57].

4. Conclusion

Polymer stabilized salt composites were successfully fabricated by impregnation of a highly porous, millimeter sized polymer matrix consisting of crosslinked pHEMA. K_2CO_3, $CaCl_2$ and LiCl were found as suitable salts to be stabilized inside the polymer matrix. The wetting behavior of the salt determines the salt distribution inside the polymer matrix. A non-wetting salt results in a homogeneous salt distribution whereas a wetting salt results in an enriched salt layer at the surface of the composite.

Composites containing wetting solutions are stable towards deliquescence in the sense that the composites retain the deliquescent solution inside the matrix. In the case of non-wetting solutions, the solution will eventually (after multiple days) leak out of the matrix.

Cyclic test using three salt-polymer composites (K_2CO_3, $CaCl_2$ and LiCl) showed that the combination of a wetting salt, while utilizing the deliquescence transition, results in the highest energy density and power output. In addition, the maximum power output was already obtained in the first cycle and found to be stable over cycling. The LiCl composite did not swell over cycles. Up to 40 deliquescence/drying cycles could be achieved until degradation of the composite occurred. To improve the cyclic lifetime a different polymer, stable to the electrolyte solution, must be used.

The manufactured composites have increased applicability for use inside an open system thermochemical reactor. The composites from this work can be made in the desired shape and size to ensure a proper permeability through the reactor bed. Something which is difficult using irregular or powder size composites. In addition, use of a composite material in a reactor bed will lower the volumetric storage density of the overall bed. Therefore, a composite material with a high MSD is

required. Due to the high (accessible) matrix porosity, composites with higher MSD were made compared to state-of-the-art literature which is expected to result in higher reactor bed densities.

This work shows a possible potential for mm-sized salt hydrate-polymer composites to be used as stable material for thermochemical energy storage. For prototype application a size/shape optimization study is required which identifies the impact of the geometry on hydration performance. In addition, in the case of deliquescent samples, a different polymer may be required exhibiting better chemical resistance. Lastly, the presented composite is suitable for open system applications. In the case of vacuum application, the thermal conductivity of the composite must be improved.

The results of this work could be expanded to other promising salts as well to improve the performance and cyclic lifetime of the desired salt hydrate.

CRediT authorship contribution statement

Joey Aarts: Conceptualization, Methodology, Writing – original draft, Visualization, Investigation. **Bas van Ravensteijn:** Conceptualization, Writing – review & editing, Investigation. **Hartmut Fischer:** Conceptualization, Writing – review & editing. **Olaf Adan:** Conceptualization, Writing – review & editing, Supervision, Funding acquisition. **Henk Huinink:** Conceptualization, Writing – review & editing, Supervision, Funding acquisition.

Declaration of Competing Interest

The authors declare that they have no known competing financial interests or personal relationships that could have appeared to influence the work reported in this paper.

Data availability

Data will be made available on request.

Acknowledgements

The authors would like to thank Hans Dalderop for his technical support and Michaela Eberbach for assisting with XRD experiments. Jouk Hamelink from Micromeritics Instrument Corporation is gratefully acknowledged for porosity measurements.

Funding

This publication is part of the Mat4Heat project with project number 739.017.014 of the research program Mat4Sus which is financed by the Dutch Research Council (NWO).

Appendix A. Supplementary data

Supplementary data to this article can be found online at https://doi.org/10.1016/j.apenergy.2023.121068.

References

[1] "Overview – World Energy Outlook 2021 – Analysis - IEA." https://www.iea.org/reports/world-energy-outlook-2021/overview [accessed Jul. 04, 2022].
[2] Sögütoglu L-C, et al. Understanding the Hydration Process of Salts: The Impact of a Nucleation Barrier. Cryst Growth Des Apr. 2019;19(4):2279–88. https://doi.org/10.1021/acs.cgd.8b01908.
[3] Lipasek RA, Li N, Schmidt SJ, Taylor LS, Mauer LJ. Effect of Temperature on the Deliquescence Properties of Food Ingredients and Blends. J Agric Food Chem Sep. 2013;61(38):9241–50. https://doi.org/10.1021/jf402585t.
[4] Lillard RS, et al. Assessment of Corrosion-Based Failure in Stainless Steel Containers Used for the Long-Term Storage of Plutonium-Based Salts. Corrosion Mar. 2009;65(3):175–86. https://doi.org/10.5006/1.3319126.
[5] Beving MAJM, Frijns AJH, Rindt CCM, Smeulders DMJ. Effect of cycle-induced crack formation on the hydration behaviour of K2CO3 particles: Experiments and modelling. Thermochim Acta Oct. 2020;vol. 692, no. March:178752. https://doi.org/10.1016/j.tca.2020.178752.
[6] van Ravensteijn BGP, et al. Encapsulation of Salt Hydrates by Polymer Coatings for Low-Temperature Heat Storage Applications. ACS Appl Polym Mater Apr. 2021;3(4):1712–26. https://doi.org/10.1021/acsapm.0c01186.
[7] Shkatulov A, Joosten R, Fischer H, Huinink H. Core–Shell Encapsulation of Salt Hydrates into Mesoporous Silica Shells for Thermochemical Energy Storage. ACS Appl Energy Mater Jul. 2020;3(7):6860–9. https://doi.org/10.1021/acsaem.0c00971.
[8] Gaeini M, Rouws AL, Salari JWO, Zondag HA, Rindt CCM. Characterization of microencapsulated and impregnated porous host materials based on calcium chloride for thermochemical energy storage. Appl Energy Feb. 2018;212(2018):1165–77. https://doi.org/10.1016/j.apenergy.2017.12.131.
[9] Casey SP, Elvins J, Riffat S, Robinson A. Salt impregnated desiccant matrices for 'open' thermochemical energy storage - Selection, synthesis and characterisation of candidate materials. Energy Build 2014;84:412–25. https://doi.org/10.1016/j.enbuild.2014.08.028.
[10] Casey SP, Aydin D, Riffat S, Elvins J. Salt impregnated desiccant matrices for 'open' thermochemical energy storage—Hygrothermal cyclic behaviour and energetic analysis by physical experimentation. Energy Build Apr. 2015;92:128–39. https://doi.org/10.1016/j.enbuild.2015.01.048.
[11] Whiting GT, Grondin D, Stosic D, Bennici S, Auroux A. Zeolite–MgCl2 composites as potential long-term heat storage materials: Influence of zeolite properties on heats of water sorption. Sol Energy Mater Sol Cells Sep. 2014;128:289–95. https://doi.org/10.1016/j.solmat.2014.05.016.
[12] Shkatulov AI, Houben J, Fischer H, Huinink HP. Stabilization of K2CO3 in vermiculite for thermochemical energy storage. Renew Energy May 2020;150:990–1000. https://doi.org/10.1016/j.renene.2019.11.119.
[13] Frazzica A, Brancato V, Caprì A, Cannilla C, Gordeeva LG, Aristov YI. Development of 'salt in porous matrix' composites based on LiCl for sorption thermal energy storage. Energy Oct. 2020;208:118338. https://doi.org/10.1016/j.energy.2020.118338.
[14] Mehrabadi A, Farid M. New salt hydrate composite for low-grade thermal energy storage. Energy 2018;164:194–203. https://doi.org/10.1016/j.energy.2018.08.192.
[15] Skrylnyk O, Courbon E, Heymans N, Frère M, Bougard J, Descy G. Performance characterization of salt-in-silica composite materials for seasonal energy storage design. J Energy Storage 2018;19(December 2017):320–36. https://doi.org/10.1016/j.est.2018.08.015.
[16] Kerskes H, Mette B, Asenbeck S, Drück H, Müller-steinhagen H. Experimental and Numerical Investigations on Thermo Chemical Heat Storage. In: *Proceedings of the EuroSun 2010 Conference, International Solar Energy Society, Freiburg, Germany*; 2010. p. 1–10, doi: 10.18086/eurosun.2010.16.14.
[17] Jabbari-Hichri A, Bennici S, Auroux A. CaCl2-containing composites as thermochemical heat storage materials. Sol Energy Mater Sol Cells Dec. 2017;172(July):177–85. https://doi.org/10.1016/j.solmat.2017.07.037.
[18] Jänchen J, Ackermann D, Weiler E, Stach H, Brösicke W. Calorimetric investigation on zeolites, AlPO4's and CaCl2 impregnated attapulgite for thermochemical storage of heat. Thermochim Acta Aug. 2005;434(1–2):37–41. https://doi.org/10.1016/j.tca.2005.01.009.
[19] Zhang YN, Wang RZ, Li TX. Thermochemical characterizations of high-stable activated alumina/LiCl composites with multistage sorption process for thermal storage. Energy Aug. 2018;156:240–9. https://doi.org/10.1016/j.energy.2018.05.047.
[20] Salviati S, Carosio F, Saracco G, Fina A. Hydrated Salt/Graphite/Polyelectrolyte Organic-Inorganic Hybrids for Efficient Thermochemical Storage. Nanomaterials Mar. 2019;9(3):420. https://doi.org/10.3390/nano9030420.
[21] Calabrese L, Hernández L, Mondragón R, Cabeza LF. Macro-porous permeability aspects of MgSO4 salt hydrate foams for energy storage applications. J Appl Polym Sci Apr. 2022;139(15):51924. https://doi.org/10.1002/app.51924.
[22] Brancato V, et al. MgSO4·7H2O filled macro cellular foams: An innovative composite sorbent for thermo-chemical energy storage applications for solar buildings. Sol Energy Oct. 2018;173(August):1278–86. https://doi.org/10.1016/j.solener.2018.08.075.
[23] Piperopoulos E, et al. Morphological and Structural Evaluation of Hydration/Dehydration Stages of MgSO4 Filled Composite Silicone Foam for Thermal Energy Storage Applications. Appl Sci Jan. 2020;10(2):453. https://doi.org/10.3390/app10020453.
[24] Calabrese L, Palamara D, Piperopoulos E, Mastronardo E, Milone C, Proverbio E. Deviceful LiCl salt hydrate confinement into a macroporous silicone foam for low-temperature heat storage application. J Sci Adv Mater Devices Sep. 2022;7(3):100463. https://doi.org/10.1016/j.jsamd.2022.100463.
[25] Pan ZH, Zhao CY. Gas–solid thermochemical heat storage reactors for high-temperature applications. Energy Jul. 2017;130:155–73. https://doi.org/10.1016/j.energy.2017.04.102.
[26] Aarts J, et al. Diffusion limited hydration kinetics of millimeter sized salt hydrate particles for thermochemical heat storage. J Energy Storage 2022;47(November 2021):103554. https://doi.org/10.1016/j.est.2021.103554.
[27] Kyle RA, Steensma DP, Shampo MA. Otto Wichterle—Inventor of the First Soft Contact Lenses. Mayo Clin Proc Mar. 2016;91(3). https://doi.org/10.1016/j.mayocp.2016.01.016.
[28] Zare M, Bigham A, Zare M, Luo H, Rezvani Ghomi E, Ramakrishna S. pHEMA: An Overview for Biomedical Applications. Int J Mol Sci Jun. 2021;22(12):6376. https://doi.org/10.3390/ijms22126376.

[29] Young C-D, Wu J-R, Tsou T-L. Fabrication and characteristics of polyHEMA artificial skin with improved tensile properties. J Memb Sci Jul. 1998;146(1):83–93. https://doi.org/10.1016/S0376-7388(98)00097-0.
[30] Kovačič S, Štefanec D, Krajnc P. Highly Porous Open-Cellular Monoliths from 2-Hydroxyethyl Methacrylate Based High Internal Phase Emulsions (HIPEs): Preparation and Void Size Tuning. Macromolecules Oct. 2007;40(22):8056–60. https://doi.org/10.1021/ma071380c.
[31] Kulygin O, Silverstein MS. Porous poly(2-hydroxyethyl methacrylate) hydrogels synthesized within high internal phase emulsions. Soft Matter 2007;3(12):1525. https://doi.org/10.1039/b711610a.
[32] Wood JM, Attwood D, Collett JH. The swelling properties of poly(2-hydroxyethyl methacrylate) hydrogels polymerized by gamma-irradiation and chemical initiation. Int J Pharm Jan. 1981;7(3):189–96. https://doi.org/10.1016/0378-5173(81)90104-6.
[33] Donkers PAJ, Sögütoglu LC, Huinink HP, Fischer HR, Adan OCG. A review of salt hydrates for seasonal heat storage in domestic applications. Appl Energy Aug. 2017;199:45–68. https://doi.org/10.1016/j.apenergy.2017.04.080.
[34] Eberbach MC, Huinink HP, Shkatulov AI, Fischer HR, Adan OCG. The Effect of Nanoconfinement on Deliquescence of CuCl 2 Is Stronger than on Hydration. Cryst Growth Des Mar. 2023;23(3):1343–54. https://doi.org/10.1021/acs.cgd.2c00821.
[35] Ritsema Van Eck GC, Chiappisi L, De Beer S. Fundamentals and Applications of Polymer Brushes in Air. ACS Appl Polym Mater 2021. https://doi.org/10.1021/acsapm.1c01615.
[36] Brunauer S, Deming LS, Deming WE, Teller E. Theory of the der Waals Adsorption of Gases 1940;62(7):1723–32.
[37] Sögütoglu LC, Donkers PAJ, Fischer HR, Huinink HP, Adan OCG. In-depth investigation of thermochemical performance in a heat battery: Cyclic analysis of K2CO3, MgCl2 and Na2S. Appl Energy Apr. 2018;215(January):159–73. https://doi.org/10.1016/j.apenergy.2018.01.083.
[38] Qian Y, Lu G, Sun Y, Song X, Yu J. Modeling of strontium chloride hexahydrate growth during unseeded batch cooling crystallization by two-dimensional population balance equation. CrstEngComm 2015;17(48):9394–403. https://doi.org/10.1039/C5CE01780G.
[39] Villars P, Cenzual K (Eds.). LiCl Crystal Structure: Datasheet from 'PAULING FILE Multinaries Edition – 2012' in SpringerMaterials (https://materials.springer.com/isp/crystallographic/docs/sd_0556891). Springer-Verlag Berlin Heidelberg & Material Phases Data System (MPDS), Switzerland & National Institute for Materials Science (NIMS), Japan, [Online]. Available: https://materials.springer.com/isp/crystallographic/docs/sd_0556891.
[40] Villars P, Cenzual K (Eds.). MgCl2·2H2O (MgCl2[H2O]2, T = 369 K) Crystal Structure: Datasheet from 'PAULING FILE Multinaries Edition – 2012' in SpringerMaterials (https://materials.springer.com/isp/crystallographic/docs/sd_1622626). Springer-Verlag Berlin Heidelberg & Material Phases Data System (MPDS), Switzerland & National Institute for Materials Science (NIMS), Japan, [Online]. Available: https://materials.springer.com/isp/crystallographic/docs/sd_1622626.
[41] Villars P, Cenzual K (Eds.). MgCl2·4H2O (MgCl2[H2O]4, T = 358 K) Crystal Structure: Datasheet from 'PAULING FILE Multinaries Edition – 2012' in SpringerMaterials (https://materials.springer.com/isp/crystallographic/docs/sd_1622625). Springer-Verlag Berlin Heidelberg & Material Phases Data System (MPDS), Switzerland & National Institute for Materials Science (NIMS), Japan, [Online]. Available: https://materials.springer.com/isp/crystallographic/docs/sd_1622625.
[42] Villars P, Cenzual K (Eds.). CuCl2 Crystal Structure: Datasheet from 'PAULING FILE Multinaries Edition – 2012' in SpringerMaterials (https://materials.springer.com/isp/crystallographic/docs/sd_0541642). Springer-Verlag Berlin Heidelberg & Material Phases Data System (MPDS), Switzerland & National Institute for Materials Science (NIMS), Japan, [Online]. Available: https://materials.springer.com/isp/crystallographic/docs/sd_0541642.
[43] Villars P, Cenzual K (Eds.). K2CO3 (K2[CO3] rt mon1) Crystal Structure: Datasheet from 'PAULING FILE Multinaries Edition – 2012' in SpringerMaterials (https://materials.springer.com/isp/crystallographic/docs/sd_1215403). Springer-Verlag Berlin Heidelberg & Material Phases Data System (MPDS), Switzerland & National Institute for Materials Science (NIMS), Japan, [Online]. Available: https://materials.springer.com/isp/crystallographic/docs/sd_1215403.
[44] Villars P, Cenzual K (Eds.). SrCl2 Crystal Structure: Datasheet from 'PAULING FILE Multinaries Edition – 2012' in SpringerMaterials (https://materials.springer.com/isp/crystallographic/docs/sd_0527498). Springer-Verlag Berlin Heidelberg & Material Phases Data System (MPDS), Switzerland & National Institute for Materials Science (NIMS), Japan, [Online]. Available: https://materials.springer.com/isp/crystallographic/docs/sd_0527498.
[45] Villars P, Cenzual K (Eds.). CaCl2 Crystal Structure: Datasheet from 'PAULING FILE Multinaries Edition – 2012' in SpringerMaterials (https://materials.springer.com/isp/crystallographic/docs/sd_1100957). Springer-Verlag Berlin Heidelberg & Material Phases Data System (MPDS), Switzerland & National Institute for Materials Science (NIMS), Japan, [Online]. Available: https://materials.springer.com/isp/crystallographic/docs/sd_1100957.
[46] Shahidzadeh-Bonn N, Azouni A, Coussot P. Effect of wetting properties on the kinetics of drying of porous media. J Phys Condens Matter Mar. 2007;19(11):112101. https://doi.org/10.1088/0953-8984/19/11/112101.
[47] Pel L, Huinink H, Kopinga K. Ion transport and crystallization in inorganic building materials as studied by nuclear magnetic resonance. Appl Phys Lett Oct. 2002;81(15):2893–5. https://doi.org/10.1063/1.1512329.
[48] Reed JJ. Digitizing 'The NBS Tables of Chemical Thermodynamic Properties: Selected Values for Inorganic and C1 and C2 Organic Substances in SI Units'. J Res Natl Inst Stand Technol Feb. 2020;125:125007. https://doi.org/10.6028/jres.125.007.
[49] Sögütoglu L-C, Birkelbach F, Werner A, Fischer H, Huinink H, Adan O. Hydration of salts as a two-step process: Water adsorption and hydrate formation. Thermochim Acta 2021;695(May 2020):178819. https://doi.org/10.1016/j.tca.2020.178819.
[50] N'Tsoukpoe KE, et al. A review on the use of calcium chloride in applied thermal engineering. Appl Therm Eng Jan. 2015;75:513–31. https://doi.org/10.1016/j.applthermaleng.2014.09.047.
[51] Yao W, Yu X, Lee JW, Yuan X, Schmidt SJ. Measuring the Deliquescence Point of Crystalline Sucrose as a Function of Temperature Using a New Automatic Isotherm Generator. Int J Food Prop Jul. 2011;14(4):882–93. https://doi.org/10.1080/10942910903474393.
[52] Fan C, Pashley RM. Precise Method for Determining the Enthalpy of Vaporization of Concentrated Salt Solutions Using a Bubble Column Evaporator. J Solution Chem Jan. 2015;44(1):131–45. https://doi.org/10.1007/s10953-014-0288-7.
[53] Lide DR. CRC Handbook of Chemistry and Physics. CRC Press; 2005.
[54] Mattsson S, Dahlström M, Karlsson S. A mild hydrolysis of esters mediated by lithium salts. Tetrahedron Lett Apr. 2007;48(14):2497–9. https://doi.org/10.1016/j.tetlet.2007.02.029.
[55] Uranta KG, Russell P, Hamad F. Determining Safe Maximum Temperature Point (SMTP) for Polyacrylamide Polymer (PAM) in saline solutions. J Oil, Gas Petrochemical Sci Jan. 2018;1(1):1–8. https://doi.org/10.30881/jogps.00004.
[56] Michel B, Neveu P, Mazet N. Comparison of closed and open thermochemical processes, for long-term thermal energy storage applications. Energy Aug. 2014;72:702–16. https://doi.org/10.1016/j.energy.2014.05.097.
[57] Ma H, et al. Strategies for enhancing thermal conductivity of polymer-based thermal interface materials: a review. J Mater Sci Jan. 2021;56(2):1064–86. https://doi.org/10.1007/s10853-020-05279-x.